Laser and Particle Beams (2008), *26*, 525–536. Printed in the USA.

doi:10.1017/S0263034608000566

Relativistic electron heating in focused multimode laser fields with stochastic phase perturbations

Y.A. MIKHAILOV, L.A. NIKITINA, G.V. SKLIZKOV, A.N. STARODUB, AND M.A. ZHUROVICH
P.N. Lebedev Physical Institute, Moscow, Russia

(RECEIVED 18 February 2008; ACCEPTED 14 July 2008)

Abstract

We describe a direct model for simulation of relativistic electrons acceleration with a given electromagnetic field which is determined by wave packet parameters. The multimode time-spatial structure of a focused Nd-laser beam with stochastic phase disturbances of each spectral component is taken into account as a source of random forces. Electron energies of more than 10 MeV are obtained even at moderate flux densities of 10^{16} W/cm^2. The developed numerical code makes it possible to obtain a quantitative energy distribution function in relation to both field intensity and the temporal bell-shape of the laser pulse. The efficient heating of electrons can be triggered in the presence of a counter propagating wave being reflected from the critical plasma area with a different reflection coefficient. The heating mechanism occurs with a delay relative to the beginning of the pulse when the laser fields exceed some threshold amplitudes. The qualitative comparison of simulation results with the experimental data is given as evidence that this mechanism is reasonable.

Keywords: Laser plasma; Relativistic electrons; Stochastic phase perturbations

INTRODUCTION

Generation of electrons in laser plasma with energy many times larger than that of the thermalized electrons is an extremely important physical phenomenon. Investigation of fast electron generation and acceleration processes in laser plasma makes it possible to understand and investigate some complicated physical processes that can accelerate electrons to very high energies (Lifschitz *et al.*, 2006; Flippo *et al.*, 2007; Mangles *et al.*, 2006; Nickles *et al.*, 2007; Niu *et al.*, 2008; Yin *et al.*, 2006). Examples of such processes are the resonant absorption of laser radiation in plasma and parametric instabilities near the critical density, two-plasmon decay in the region of the quarter-critical density, stimulated Raman scattering in plasma coronas, and discussed in this report relativistic electron heating in focused multimode laser fields with stochastic phase perturbations (Bret *et al.*, 2006, 2007). From the practical point of view, it is very promising to use a laser plasma that generates fast electrons as the cathode of an injector of high-current pulsed accelerators since such laser-plasma cathodes can, compared with traditional types of cathodes, ensure a high initial energy of the electrons ($>10^2$ keV), a short duration of the injection pulse ($<10^{-9}$ s), and huge current densities ($>10^6$ A/cm^2). The generation of fast electrons in a laser plasma can play a very important role for the purposes of laser thermonuclear fusion (Nakamura *et al.*, 2006; Sakagami *et al.*, 2006). In schemes of hydrodynamic acceleration and compression of thermonuclear targets, even a small number of high-energy electrons, carrying less than 1% of the absorbed laser energy penetrating into the central region of the target can cause it to be preheated, and thereby catastrophically lower the compression by more than an order of magnitude, and prevent the attainment of the necessary value of the confinement parameter ρR (ρ, R—are the density and radius core of a target). On the other hand, the positive role of high-energy electrons is very important in the scheme of laser thermonuclear fusion known as "fast ignition" (Badziak *et al.*, 2006; Hora, 2007; Yu *et al.*, 2007; Zvorykin *et al.*, 2007). In many experimental works, high-energy electrons have been observed. The presence of hot electrons resulted in appearance of high energetic ions and anomously hard X-ray emission spectrum. The most recent papers dealt with hot electron observation are concerned with laser plasma produced by femtosecond laser radiation focused onto solid target at flux densities of 10^{18}–10^{20} W/cm^2 (Chen & Wilks, 2005). The relativistic factor is much more than unity at such radiation densities. There are a few

Address correspondence and reprint requests to: Y.A. Mikhailov, P.N. Lebedev Physical Institute, Moscow, Russia. E-mail: mikh@sci.lebedev.ru

experiments in the range of $10^{13}-10^{15}$ W/cm^2 and at nanosecond pulse duration in which anomalously energetic electrons (essentially more than oscillatory energy) were registered. The most important is the fact that the significantly large part of incident laser energy was converted into energy of hot electrons. In a number of works, the different stochastic acceleration mechanisms were considered to explain anomalous energy of electrons when spontaneous self generated magnetic fields or plasma wave beating or wake fields were used as a source of random perturbation of momentum of an electron. See for example, Ivanov *et al.*, 1996, 1995; Key *et al.*, 1998; Sheng *et al.*, 2004; Sentoku *et al.*, 2002. Laser energy transfer and enhancement of plasma waves and electron beams by interfering high-intensity laser pulses were considered (Zhang *et al.*, 2003). One of the first publications with experimental data on super fast electrons generated in laser plasma was Rousseaux *et al.* (1992). In this work, electrons with energy up to 1 MeV produced in laser-plasma interactions at 0.26, 0.53, and 1.05 μm laser wavelength have been measured. The laser radiation on the foil target surface was around 10^{15} W/cm^2. In the work by Gibbon (1994), interesting theoretical results on high-energy electrons generation have been received at an irradiation of solid-state targets by laser radiation with femtosecond duration. The flux density on the target surface was $q \approx 10^{17}$ W/cm^2 at the wavelength $\lambda = 1$ μm. The values of energy ("temperature") received in hydrodynamic calculations from 250 keV to 360 keV coincide with values of energy at the initial stages of picoseconds laser pulse considered in our work.

In the present paper, we consider a mechanism of stochastic electron heating under critical homogeneous electron density and at focal intensities in the range of $10^{13}-10^{17}$ W/cm^2 which are important for direct fusion target heating. The field random phase distribution over focal plane (speckle structure of intensity) as well as phase beating in wave packet of multimode Nd-laser beam of 3 ps duration are taken into account as a source of random forces in equation of motion of a charged particle. The dependence of electron energy distribution function shape and dependence of mean energy on focal intensity was obtained numerically. The calculation of trajectories of 2000 electrons resulted in their directivity at output equaled to ~0.7 rad. The reflected from critical area wave was taken into account.

INTENSITY AND FIELD DISTRIBUTION IN THE FOCAL PLANE

The focal intensity distribution was measured for aspherical lens with focus 10 cm and aperture of the beam 45 mm. In Figure 1, experimental intensity distribution in arbitrary units at the focal plane is shown. Laser pulse duration is ~2 ns. The speckle structure slightly varies from shot to shot. Nevertheless, the character of image preserves the same. In the case of 2 ps duration (the energy ~0.5 J), the picture of intensity distribution was like one for 2 ns pulse on the whole. It is seen that the spatial position of speckles has random character. The scale of Y-Z plane is in microns. We use about 80 modes of laser radiation to construct field intensity distribution, which corresponds to experimental data of radiation intensity distribution as shown in Figure 1. The field intensity amplitude distribution calculated in focal plane is given in Figure 2. In the process of preselection of suitable mode structure of wave packet to compare calculated intensity distribution with experimental one, we did not take into account longitudinal component of E, H-fields, which can be estimated about 10–15% of perpendicular one. Total accuracy of such reconstruction of E, H-fields was in the limits of 10–20%. Random depolarization up to 20% does not influence on the reconstruction with such accuracy. Then we reconstruct field distribution numerically by choosing the structure of beam which corresponded to the focal intensity. We use an angle structure consisting of several tens of angular modes, so the total divergence was about 2×10^{-4} rad. In Figure 2, field intensity distributions are

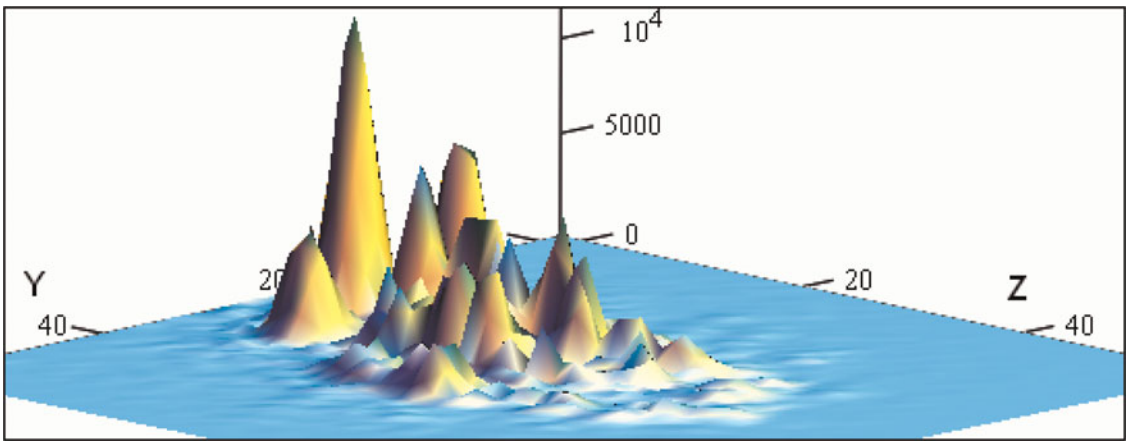

Fig. 1. (Color online) Typical focal intensity distribution experimentally measured at flux density ~10^{14} W/cm^2. The scale of Y-Z plane is in microns.

https://doi.org/10.1017/S0263034608000566 Published online by Cambridge University Press

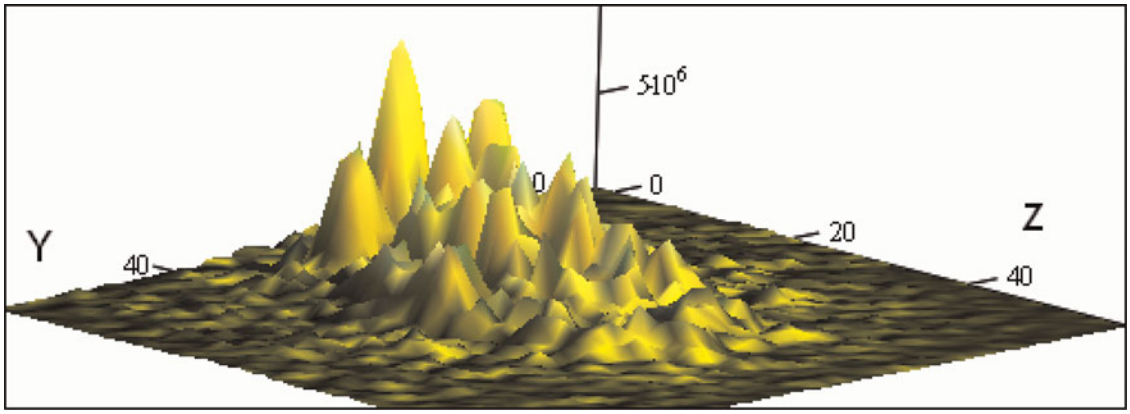

Fig. 2. (Color online) Typical field intensity distribution reconstructed for multimode radiation to be corresponded approximately to intensity distribution shown in Figure 1. The scale of Y-Z plane is in microns.

given for focal Y-Z plane (the same scale). The common behavior of focal intensity distribution as shown in Figure 1 for 2 ns laser pulse does not strongly differ from the distribution measured for 2 ps laser pulse (at energy of 35 J).

Polarized E-field phase distribution is shown in Figures 3 and 4. The mean distance between phase speckles is on the order of a few microns. If we consider an electron moving with relativistic velocity in the focal region, it will pass across areas with a stepwise change of field phase. The frequency of intersection by the electron of phase speckle areas is comparable with the frequency of heating light.

For illustration in Figure 4, there are the field phase traces for two perpendicular cross sections, $y = 0$ or $z = 0$. Note that the phase changes randomly over the Y–Z plane in the limits from π to $-\pi$. The relative phase shift between two successive maximum and minimum of E-field is shown. The absolute phase shift there is defined with the accuracy of $2\pi \times r$, where n is an integer. One can see that the phase step changes from speckle to speckle randomly both in amplitude and in spatial derivative of phase variation. It enables us to comprehend random terms in the phase of light wave to simulate the action of electromagnetic fields onto moving electron in different phase speckle areas. To facilitate the computations, we approximated the traces shown in Figure 4 by rectangular ones with fixed frequency and with amplitudes randomly changing from step to step. The maximum random variation of phase is about 2π in this case.

THE MODEL

The model describes the acceleration of charged test particles in a given electromagnetic field formed in focal area by polarized incident and reflected light beams. The incident and reflected beams consist of a few frequency components each. The complicated phase structure of focal intensity speckle patterns was approximated by regular phase perturbation in time with random phase shock amplitude. The frequency of phase shocks, which electron meets along its motion trajectory, corresponds to two-third of the critical plasma frequency. A moving electron experiences an electromagnetic field the phase of which changes sharply in a time rather less than wavelength period. Then the phase is constant

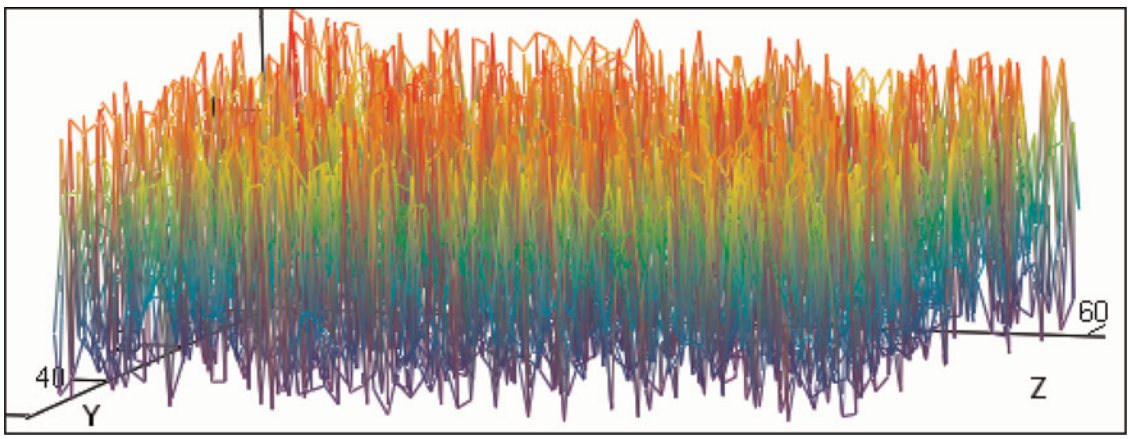

Fig. 3. (Color online) Two-dimensional electric field phase distribution over the focal Y-Z plane. The scale of axes is the same as in Figure 2.

https://doi.org/10.1017/S0263034608000566 Published online by Cambridge University Press

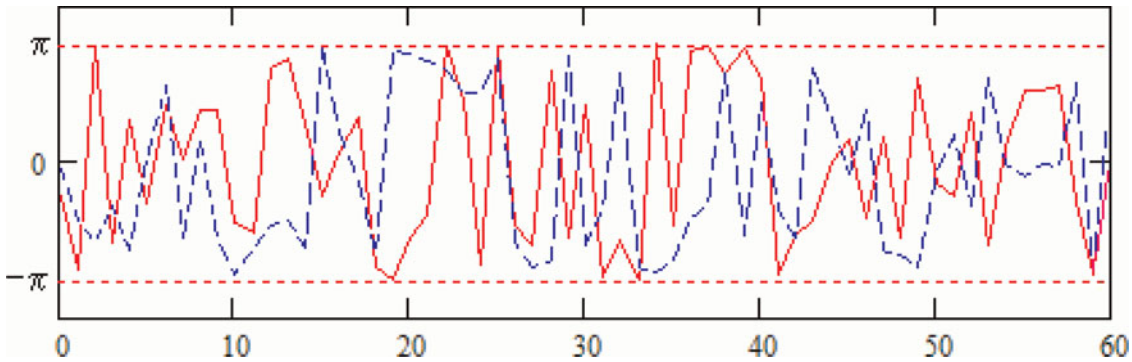

Fig. 4. (Color online) Field phase traces over focal plane for two perpendicular cross sections, $y = 0$ (solid) or $z = 0$ (dashed).

until the next phase jump occurs. The random spread of relative phase of each spectral component was taken into account. The temporal shape of laser beam wave packet was U-shape, which approximate by envelope function $\delta(t) = [(1 - t/\tau) \cdot t/\tau]$. The multicomponent spectral line of laser radiation approximated by the function

$$f(j) = \left(1 - \frac{j}{N_L}\right) \times \frac{j}{N_L},$$

where j is the component number and N_L is the number of components. For example, Nd-glass radiation usually consists of 12 spectral components. However, in this work, we consider only four components to simplify and quicken numerical procedure. The phase factor of a component is represented by expression

$$f_e(j, t) = \exp\left(i \times \left[\omega_0 \left[1 + \left(\frac{\Delta n_\lambda}{n_\lambda}\right) \times \left(j - \frac{N_L}{2}\right)\right] \times \left(t - \frac{\tau}{2}\right) - \Phi_j\right]\right) \times f(j),$$

where ω_0 is the frequency at the maximum of spectral line, n_λ is the number of periods in pulse duration (τ), Δn_λ is the frequency interval in number of periods between neighboring equidistant spectral components, and Φ_j is the random phase but not more than it follows from uncertainty condition. For example, in the case of polarized field, we can write

$$E_y(\vec{r}, t) = A(y, z) \times \left(\sum_{j=0}^{N_L} f_e(j, t)\right) \times \left[(1 - \gamma) \times e^{-ik_x x} + 2\gamma \cos k_x x\right] \times \delta(t) \cdot e^{i\psi(t)},$$

$$H_z(\vec{r}, t) = A(y, z) \times \left(\sum_{j=0}^{N_L} f_e(j, t)\right) \times \left[(1 - \gamma) \times e^{-ik_x x} - 2i\gamma \sin k_x x\right] \times \delta(t) \cdot e^{i\psi(t)},$$

where $k_x \approx 2\pi/\lambda$ is the wave number, $\psi(t)$ is the random function, and $\gamma = E_{refl}/E_{inc}$ is the amplitude reflection coefficient. The longitudinal and depolarization parts of fields are written by the similar way. They does not influence essentially on the electron stochastic motion at least on the level of 20% of field amplitude. In our model, spatial nonuniformity of a field does not influent a great deal on energy gain in contrast to work (Maiorov *et al.*, 2004).

STOCHASTIC EQUATIONS OF MOTION

To investigate the acceleration of test particles in the electromagnetic fields formed as described above, we consider the relativistic equations of motions of a positive electron in a given external electromagnetic field:

$$\frac{d\vec{r}'}{dt'} = v'(\vec{p}'); \frac{d\vec{p}'}{dt'} = \frac{q}{c} \cdot \vec{v}'(\vec{p}') \times \vec{B}(\vec{r}', t') + q \cdot \vec{E}'.$$

Here are unknown variables: p'_x, p'_y, p'_z, x, y, z, here the dotted values related to real values. For the numerical integration, we express equations in terms of the following relations: $t = ct'$, $\vec{p} = \vec{p}'c/mc^2$, $T_{kin} = T'_{kin}mc^2$, $\vec{V} = \vec{V}'/c$, $E = qE'/mc^2$, $B = qB'/mc^2$. Now we write the reduced equations in the form:

$$\begin{cases} \frac{d\vec{r}}{dt} = \vec{\beta}(\vec{p}), \vec{\beta}(\vec{p}) = \frac{\vec{p}}{\sqrt{1 + (\vec{p} \cdot \vec{p})}}, \\ \frac{d\vec{p}}{dt} = \vec{\beta}(\vec{p}) \times \vec{B}(\vec{r}, t) + \vec{E}(\vec{r}, t). \end{cases}.$$

Here time t is expressed in cm. Coordinates x, y, z are unchangeable, and are expressed in cm. The reduced energy T and momentum p_x, p_y, p_z assigned in units of electron rest energy mc^2. The particle motion equations are solved with a fourth order Runge-Kutta adaptive step-size scheme. In numerical calculations, we analyze the motion of 1000–2000 free electrons. The laser pulse duration is ~3.5 ps, which is appropriate to 1000 wavelengths. The pulse shape was approximated by parabola function $\delta(t)$ with high contrast ratio which is rather different from Gauss shape. The electrons gain the most energy only in the X-Y plane in spite of the three-dimensional (3D)

https://doi.org/10.1017/S0263034608000566 Published online by Cambridge University Press

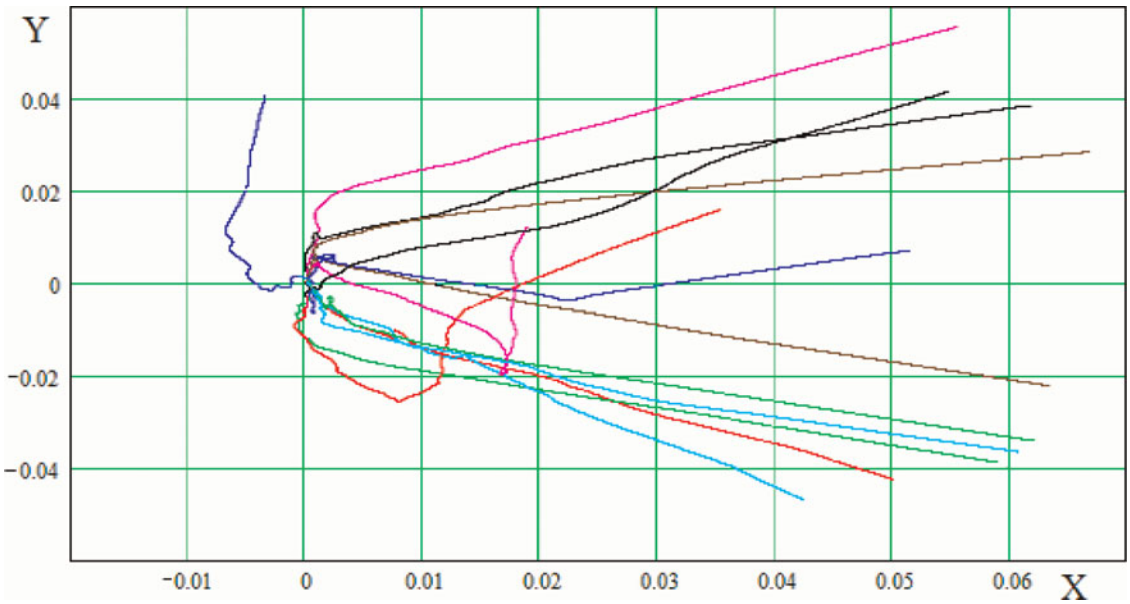

Fig. 5. (Color online) Trajectories projected on to X-Y plane for typical test electrons. X [cm] is parallel to wave vector $\vec{k}$; Y [cm] parallel to E field. The fourteen curves are taken by an arbitrary way.

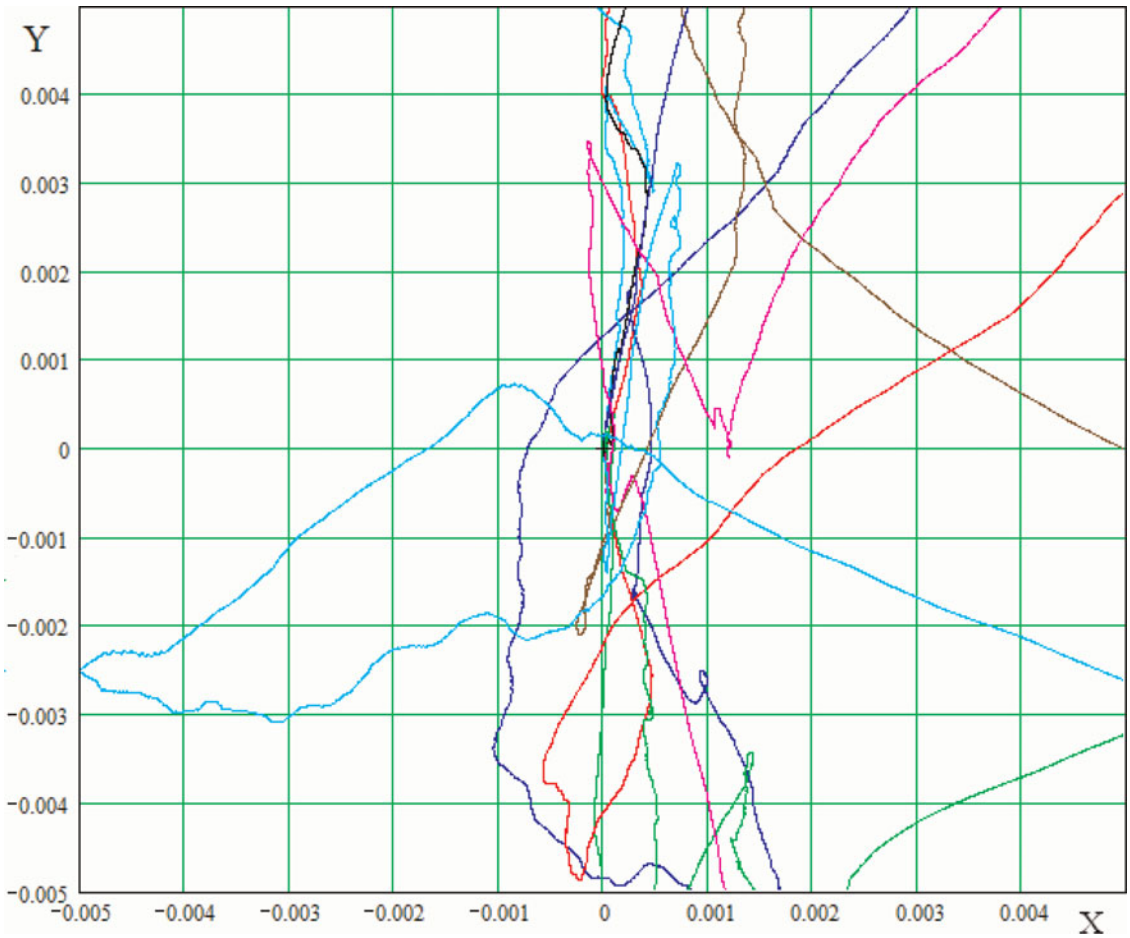

Fig. 6. (Color online) The early stage of a particle trajectory. Typical length of a trajectory in this spatial area corresponds to about 20% of the front of laser pulse. X [cm] is parallel to wave vector $\vec{k}$; Y [cm] is parallel to E field.

https://doi.org/10.1017/S0263034608000566 Published online by Cambridge University Press

trajectory. We consider the uniform neutral cloud of non-intaracting electrons in spatially and time modulated electromagnetic fields. The test electrons start acceleration within the simulation box at random positions. Momentum initial conditions corresponded to normal distribution with temperature of ~0.5 keV, which represents a typical value in laser plasma corona near critical area for focal intensities under consideration in this work. The simulations were performed with a resolution of 50 cells per laser wavelength and time step was carefully chosen to ensure that numerical dispersion was not a factor.

In this model, we consider the cause of appearance of supra energetic electrons, which produce positive space charge in a plasma after they escape it. The total number of such electrons is determined by the potential of plasma cloud that is by its finite size and by mean energy of escaping electrons. In other words, the calculations of electrons energy distribution function and current density of electrons, which gives us possible to evaluate the scale of macroscopic E-field intensity (plasma potential) have been made in this work.

THE ELECTRON TRAJECTORIES

Figures 5 and 6 illustrate absolutely stochastic motion of electrons in random electromagnetic field. Especially it is seen in Figure 6. In Figure 5, a set of trajectories projected onto X-Y plane of typical test electrons is shown. The end of a trajectory is consistent with the end of the wave packet subsequent to electromagnetic fields are switched off. It can be seen that during irregular motion, a particle is subjected to a random force than stronger than its momentum is lower. When a stochastic acceleration is developed, the motion of particles becomes directional. The most part of electrons moves in the direction of incident wave

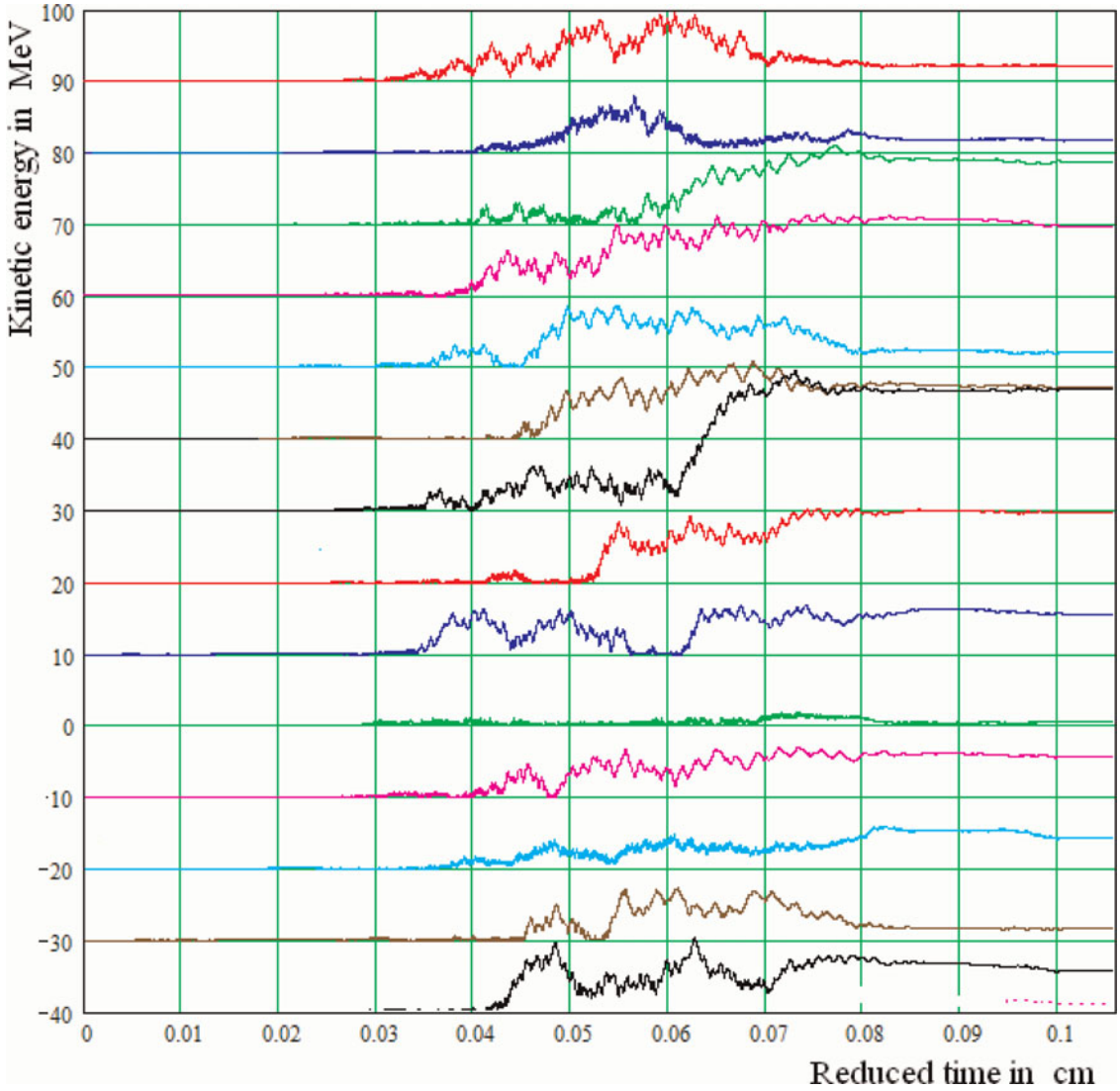

Fig. 7. (Color online) The time evolution of the kinetic energy of fourteen arbitrary test electrons for fixed field intensity corresponded to light intensity $q = 2 \times 10^{17}$ W/cm^2. Each cell in vertical axis is equal to 10 MeV for corresponding curve. Pulse duration is 3.5 ps.

https://doi.org/10.1017/S0263034608000566 Published online by Cambridge University Press

propagation. It is notable that about half of the particles move inside the angle of ~0.7 rad (in the case of 2000 particle trajectories analysis). In the case of long pulses of 3.5 ps and 10 ps duration, the directivity of particle motion does not depend on initial phase position that is on the random initial position in simulation box. The same regards to random initial energy of a particle. This fact confirms the stochastic nature of motion under electromagnetic field phase perturbation. In this case, electric field E_y and magnetic field B_z were polarized. The longitudinal components of the electromagnetic field have not been taken into account. The small depolarization ~5% does not influence on the trajectories a great deal. Each incident field consists of two frequency components with frequency interval $\Delta\omega = \omega_0/500$ and with random relative phase. The reflection coefficient was equal to $\gamma = 0.2$. When reflection is close to unity $\gamma > 0.8$, the electron motion reminds one of the cases of standing wave. The directivity of electron motion to the end of the pulse there with becomes almost isotropic.

In the Figure 6, the early stage of particle acceleration at the beginning of laser pulse duration is shown when the energy of a particle is still less than the relativistic one. A particle in this figure experienced the two-dimensional (2D) action of about 10–20 periods of light field. The further stochastic motion (Fig. 5) does not depend on directivity at initial stage when the motion is not relativistic. The directivity is formed when the energy of a particle is more than or close to relativistic energy. This fact follows from the analysis of 1000 trajectories. It is easy to see that the initial stage of motion of a particle strongly dependent on random initial energy and space phase position in simulation box. However, at the early times that are a few tens of wave periods, the increase of stochastic energy of a particle is not noticeable. The direction of initial particle moving is dependent on random initial phase and the values of momentum components. In some cases, a long linear part of trajectory can be seen that implies to the minimum of magnetic field in the point of initial position of a test particle.

THE ENERGY GAIN OF A PARTICLE DURING LASER PULSE

In Figure 7, the time evolution of the kinetic energy of a test electron for fixed field intensity corresponded to light intensity $q = 2 \times 10^{17}$ W/cm^2 is shown. There are typical 14 arbitrary selected traces from 1000 ones. Initial conditions are as mentioned above. The time [in cm] is plotted on X-axis. A vertical division is equaled to 10 MeV for each trace. The field is switched off at 0.1 cm for convenience of observation. It is easily seen that stochastic process of particle acceleration

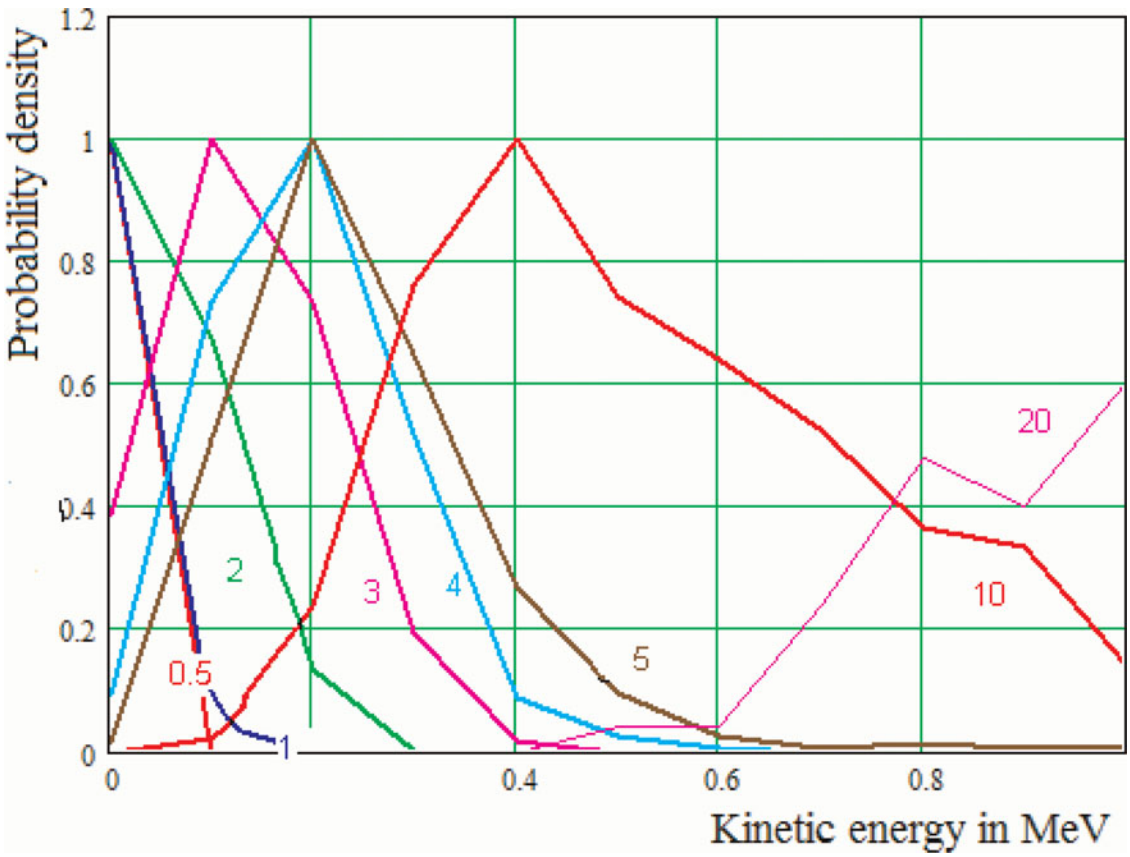

Fig. 8. (Color online) The distribution functions of electrons normalized to the maximum probability for different field intensities. Numerals near the curves denote distribution functions corresponding to field intensity parameter *eb*.

https://doi.org/10.1017/S0263034608000566 Published online by Cambridge University Press

develops after some delay, which varies from tens to hundreds of wavelengths. This delay is longer than for the case of rectangular pulse when the field switched on instantaneously. The damping of small variations is related to the decrease of field intensity on the slope of the pulse. The small structures of an energy evolution trace account for force perturbations, which resulted in the change of direction of the momentum of a test particle. The stochastic character of kinetic energy growth during acceleration by strong electromagnetic wave with randomly phase variation is illustrated by this figure as well as it can be seen from stochastic movement of an electron trajectory shown in Figure 6.

ENERGY SPECTRUM OF ELECTRONS

In Figure 8, the distribution functions of electrons normalized to the maximum probability for different field intensities are presented. The figure denoted by "mean" implies to the energy averaged over a proper curve. The parameter *eb* implies the value of field intensity in terms of Mega CGSE/cm. For example, $eb = 20$ is matched to power density of $q = 10^{17}$ W/cm^2. The parameter $eb = 0.5$, 1, 2, 3, 4, 5, 10, 20 in Figure 8 denote distribution functions corresponding to field intensities equaled to 6×10^{13}, 2.5×10^{14}, 2.5×10^{15}, 2×10^{15}, 4×10^{15}, 5.2×10^{15}, 2.5×10^{16}, 2×10^{17} W/cm^2. The energy distribution functions are not Maxwellian, they have a long energetic tail.

In Figure 9, the curves denoted by "output energy probability" correspond to energy distribution functions of electrons at the end of the laser pulse ~3.5 ps. The curves "cutoff energy probability" shows the fractional number of electrons having the energy more than corresponding figure on X-axis. The curves "cutoff current" show the normalized current, which can be registered by a detector outside interaction area. It can be seen from these graphs that at flux density 2×10^{17} cm^2 more than 20% of electrons can have energies more than 6 MeV. Here "output energy probability" means energy distribution of 1000 electrons at time equaled to 90% of pulse duration. The "cutoff energy probability" means the fraction of particles having energy which exceeds the corresponding value on X-axis. The "cutoff current" means the fractional current value of electrons

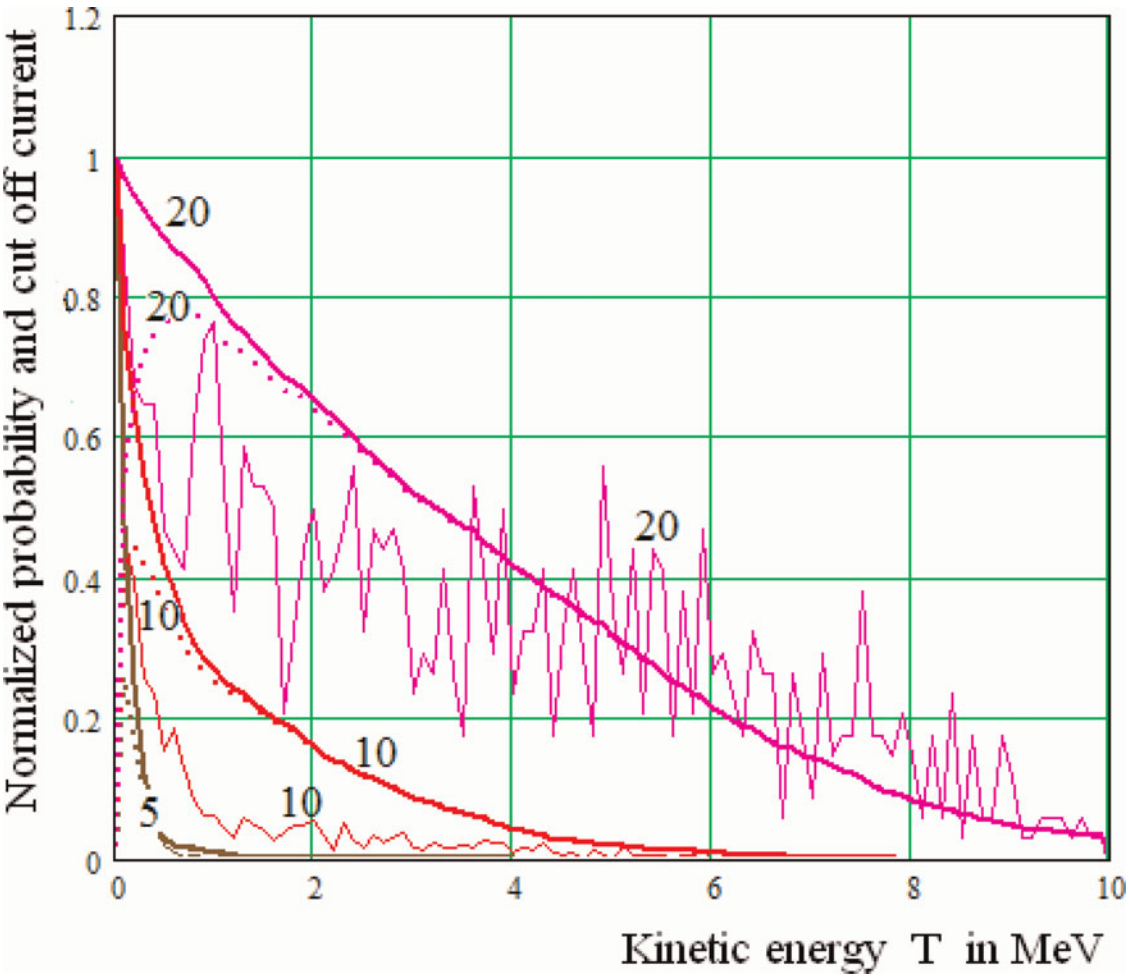

Fig. 9. (Color online) Energy distribution functions of electrons at the end of the laser pulse ~3.53 ps (solid thin curves). Cutoff energy probability (solid thick curves). Normalized cutoff current (dotted curves). Numerals near the curves denote field intensity parameter *eb*.

https://doi.org/10.1017/S0263034608000566 Published online by Cambridge University Press

which escape focal area and have the energy more than the value on X-axis one. The parameter *eb* indicates the value of field intensity in units of 10^6 CGSE $= 3 \times 10^8$ V/cm. The dotted curves designated by "cutoff current" show the probability of total flow of particles which escape the interaction area. It is really electric current which can be measured like it was done in previous work at intensities 10^{13}–10^{15} W/cm^2. Curves "cutoff energy probability" show the fractional number of particles which have energy more than the energy on X-axis. At flux density $q = 10^{17}$ W/cm^2 ($eb = 20$), the energy distribution function is not smooth, which is not simply explainable. We can say only that this is not associated with numerical procedure at least in the framework of approximation model given above. The data given in Figure 9 result in large amount of electrons which have energy rather more than relativistic oscillatory energy. For example, the fractional part of electrons which have energies more than 350 keV is equal to ~15% even at relatively low intensity $\sim 6 \times 10^{15}$ W/cm^2, and the same 15% part of electrons have energies more than 2 MeV at intensity $\sim 2 \times 10^{16}$ W/cm^2. These curves were obtained by processing of 2000 electrons trajectories which were calculated with 80 cells per wavelength ($\lambda = 1.60$ μm).

DISCUSSION

In Figure 10, we attempt to compare the simulation results with experimental data. For comparison with experiment, the data from Ivanov *et al.* (1996) were used. In this work, the original techniques for investigation of superfast electrons in laser plasma have been used. The method was based on direct measurements of electron emission allowing to obtain data on maximum electron cutoff energy and to measure integrated values of their currents. Experiments were carried out at the installation "PICO" in the Laser Plasma Laboratory of P. N. Lebedev Physical Institute. The installation consists of two lasers (nanosecond and picosecond ranges of laser pulse duration). Nd-laser radiation ($\lambda = 1.06$ μm) from the master oscillator was amplified in the laser cascades and was focused on a target placed in the vacuum chamber with residual pressure of air $\sim 10^{-5}$ torr. Duration of a light impulse was supervised by a

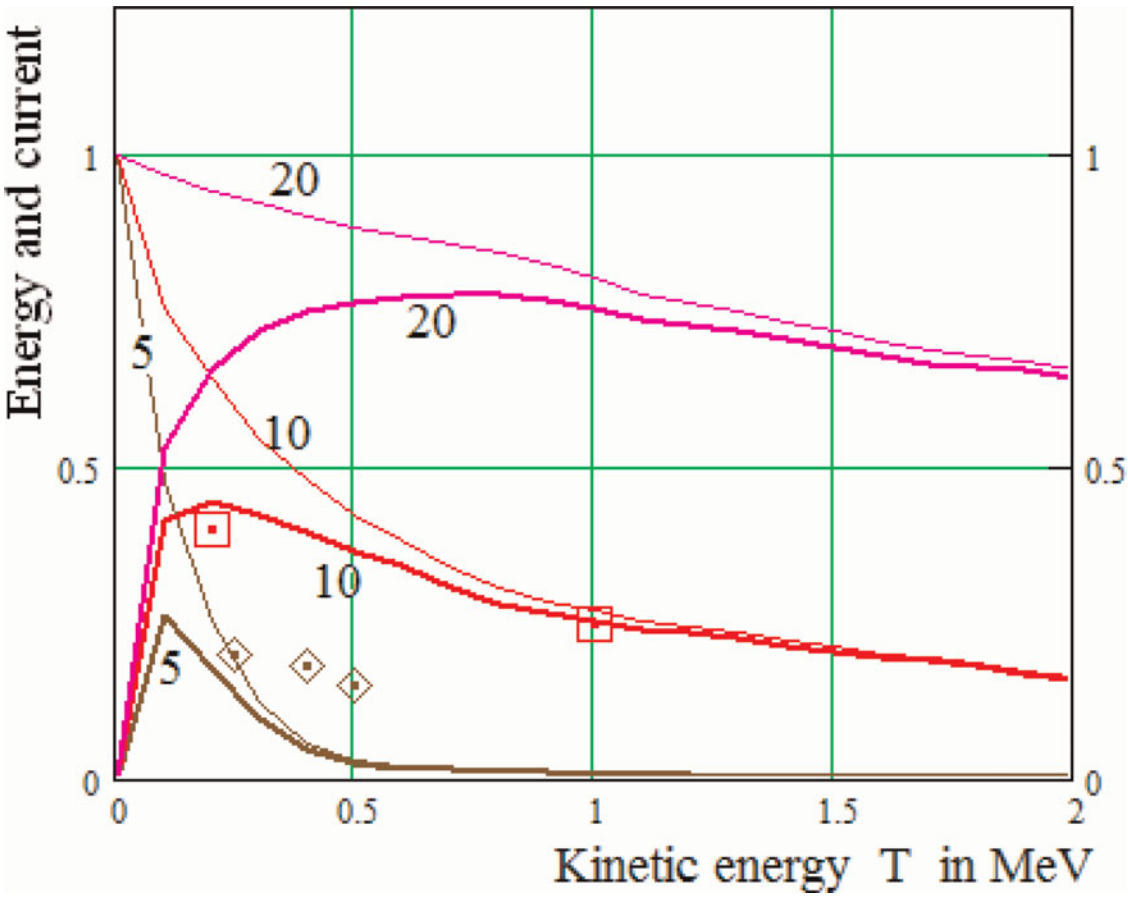

Fig. 10. (Color online) Comparison of the simulation results with experimental data. Normalized cutoff current calculated using distribution functions shown in Figure 8 (solid bold curves). Cutoff energy probabilities are shown for illustration (solid thin curves). Numerals near the curves denote field intensity parameter *eb*. Experimental data are given for two laser intensities: diamonds (◇) correspond to $eb = 5$; boxes (□) correspond to $eb = 10$.

https://doi.org/10.1017/S0263034608000566 Published online by Cambridge University Press

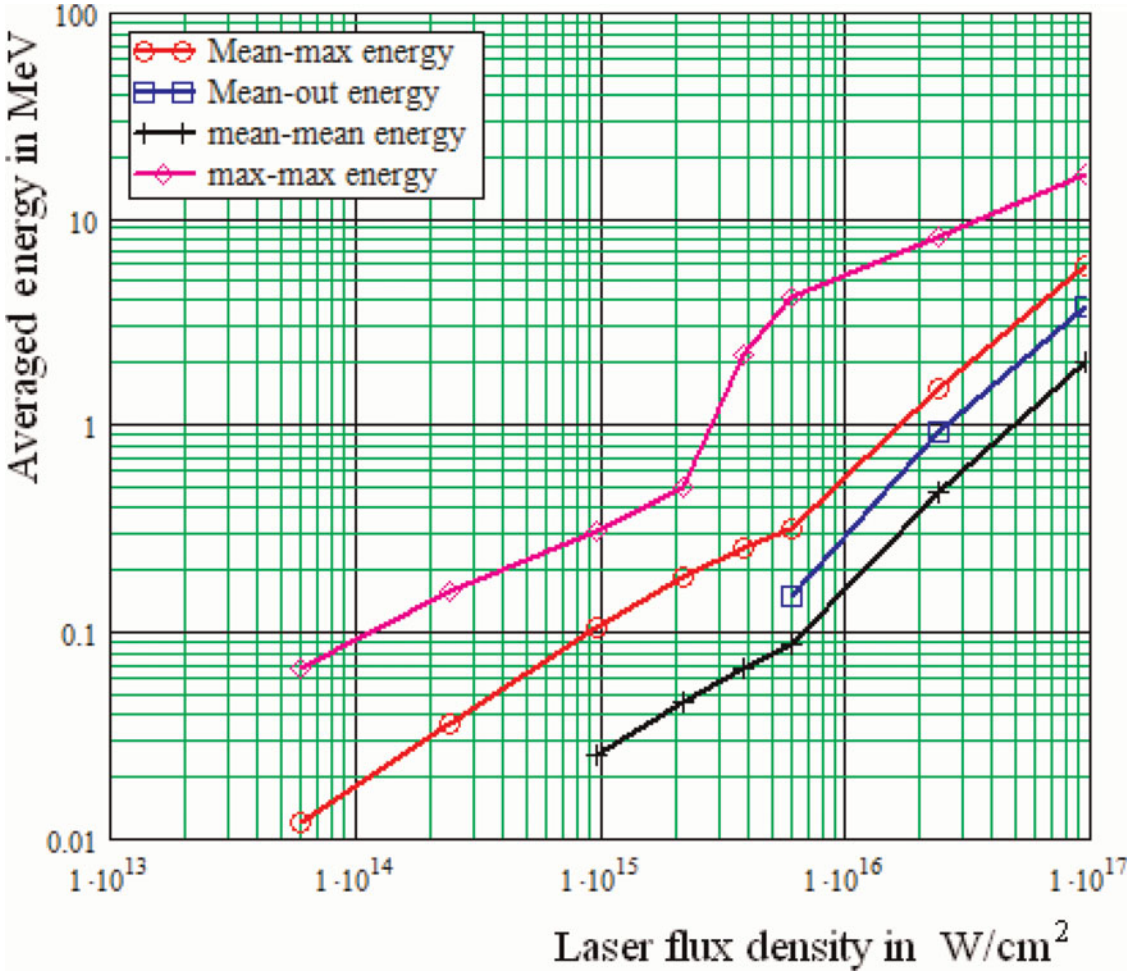

Fig. 11. (Color online) The dependence of maximal energy on intensity (diamonds). The dependence of maximal energy during pulse averaged over 2000 electrons on intensity (circles). The averaged energy of the electrons at the end of the pulse (boxes). The electron energy averaged over all electrons and averaged over the pulse for each electron (crosses).

coaxial photo cell and was $\tau \approx 2$ ns. Energy of laser radiation varied in a range of 1–20 J and was measured by means of calorimeters. The divergence of laser radiation was $\alpha \approx 1 \times 10^{-4}$ rad. The energy contrast ratio of laser radiation on the target was $K_E \approx 10^5$–10^6 with of a spectrum bandwidth $\Delta\lambda = 30$ Å. The focusing system with aspherical optics allowed to irradiate a target with power density on a target surface in a range 10^{12}–8×10^{13} W/cm^2 in experiments on nanosecond laser and up to 10^{16} W/cm^2 for picosecond experiments.

The target was a coaxial capacitor sensor and was consisted of actually target in the form of a cylindrical core with Ø5 mm and the length 10 mm located in a cylindrical cover. The space between a target and a cover was filled with an insulator (Teflon with the thickness ~200 μm). Proposed method allowed us to measure the whole number of electrons from the target which have the energy more then a given fixed value.

Oscilloscope measurements have allowed measuring the maximum cutoff energy of super fast electrons. The estimation of electron current density from plasma was $j \sim 7 \times 10^{14}$ A/cm^2. The experimental points were obtained by measuring total cutoff electron current from a copper solid target. The cutoff current is expressed by $j_{cutoff} = \int_T^\infty w(T) \times \sqrt{T(T+2)}/T + 1 dT$, where $w(T)$ is the electron energy distribution function. Here, the two diamonds correspond to intensity ~10^{16} W/cm^2 which measure as averaged over focal spot and in time. Indeed there are spikes of intensity a few times more than averaged intensity. So these points can be compared with the red curve calculated at intensity 2.5×10^{16} W/cm^2. The three brown diamonds were measured at focal intensity ~10^{14-15} W/cm^2. We try to comply these points with the brown curve which calculated at intensity 6×10^{15} W/cm^2. The bold curve for the current was calculated at intensity 10^{17} W/cm^2 ($eb = 20$). It illustrates that half of electrons gain energy more than 3 MeV. Qualitatively it is not contradictory to results obtained experimentally with femtosecond pulses. But quantitative comparison is not possible. Nevertheless the model in which random phase perturbation of focal field phase is taken into account can be considered a

https://doi.org/10.1017/S0263034608000566 Published online by Cambridge University Press

real possibility to explain the appearance of anomalously energetic electrons in laser plasma at moderate intensity density. It is notable that up to 30% of absorbed laser energy was converted in electrons with mean energy exceeding 600 keV at 0.5 ps, 15 J, $\sim 10^{19}$ W/cm^2 (Key *et al.*, 1998), and up to 30% of absorbed laser energy was the energy of target charge due to 300 keV electrons at 2 ns, $\sim 10^{14}$ W/cm^2 and 3.53 ps, $\sim 10^{15}$ W/cm^2 pulses (Ivanov *et al.*, 1996).

The processing of data obtained by simulation resulted in dependence of electron energies on focal laser power density which is consistent with our theoretical model. The four curves are shown in Figure 11 where in X-axis the intensity and in Y-axis energy are plotted in absolute units. The upper curve (diamonds) shows the dependence of maximal energy on intensity. The next lower curve (circles) shows the dependence of maximal energy during pulse averaged over 1000 electrons on intensity. The next lower curve (boxes) related to averaged energy of the electrons at the end of the pulse. Finally the lowest curve (crosses) related to electron energy averaged over all electrons and averaged over the pulse for each electron.

It is possible to introduce some effective characteristic "temperature" T_{eff} of high energy electrons appeared as a result of stochastic acceleration. It is reasonable to apply as this "temperature" the energy averaged over pulse duration and over all electrons as well. Thus the lowest curve shows the dependence of such temperature on laser flux density. In the range of intensities 6×10^{13} to 6×10^{13} W/cm^2 the dependence looks like $T_{eff} \sim q^{0.45-0.55}$ at wavelength $\lambda = 1.06$ μm. In the range of higher intensities 6×10^{15} to 6×10^{17} W/cm^2 the power increases as $T_{eff} \sim q^{0.8-0.9}$. Thus than intensity density of laser radiation approaches to relativistic one than the power of this dependence becomes more close to unity.

ACKNOWLEDGEMENTS

Authors would like to thank V. V. Klimov and V. V. Okorokov for useful discussions. This work was supported by Russian Foundation for Basic Researches under Project No. 08-02-00913-a.

REFERENCES

Badziak, J., Glowacz, S., Hora, H., Jablonski, S. & Wolowski, J. (2006). Studies on laser-driven generation of fast high-density plasma blocks for fast ignition. *Laser Part. Beams* **24**, 249–254.

Bret, A., Firpo, M.C. & Deutsch, C. (2006). Between two stream and filamentation instabilities: Temperature and collisions effects. *Laser Part. Beams* **24**, 27–33.

Bret, A., Firpo, M.C. & Deutsch, C. (2007). About the most unstable modes encountered in beam plasma interaction physics. *Laser Part. Beams* **25**, 117–119.

Chen, H. & Wilks, S.C. (2005). Evidence of enhanced effective hot electron temperatures in ultraintense laser-solid interactions due to reflexing. *Laser Part. Beams* **23**, 411–416.

Flippo, K., Hegelich, B.M., Albright, B.J., Yin, L., Gautier, D.C., Letzring, S., Schollmeier, M., Schreiber, J., Schulze, R. & Fernandez, J.C. (2007). Laser-driven ion accelerators: Spectral control, monoenergetic ions and new acceleration mechanisms. *Laser Part. Beams* **25**, 3–8.

Gibbon, P. (1994). Efficient production of fast electrons from femtosecond laser interaction with solid targets. *Phys. Rev. Lett.* **73**, 664–667.

Hora, H. (2007). New aspects for fusion energy using inertial confinement. *Laser Part. Beams* **25**, 37–45.

Ivanov, V.V., Knyazev, A.K., Kutsenko, A.V., Matsveiko, A.A., Mikhailov, Yu.A., Osetrov, V.P., Popov, A.I., Sklizkov, G.V. & Starodub, A.N. (1996). Investigation of the generation of high-energy electrons in a laser plasma. *JETP* **82**, 677–682.

Ivanov, V.V., Knyazev, A.K., Kutsenko, A.V., Matsveiko, A.A., Mikhailov, Yu.A., Osetrov, V.P., Popov, A.I., Sklizkov, G.V. & Starodub, A.N. (1995). Method of fast electron observation in laser plasma. *Prib. Tekn. Eksp.* **4**, 112–116.

Key, M.H., Campbell, E.M., Cowan, T.E., Hatchett, S.P., Henry, E.A., Koch, J.A., Langdon, A.B., Lasinski, B.F., MacKinnon, A., Offenberger, A.A., Pennington, D.M., Perry, M.D., Phillips, T.J., Sangster, T.C., Singh, M.S., Snavely, R.A., Stoyer, M.A., Tsukamoto, M., Wharton, K.B. & Wilks, S.C. (1998). The potential of fast ignition and related experiments with a petawatt laser facility. *J. Fusion Energy* **17**, 231–236.

Lifschitz, A.F., Faure, J., Glinec, Y., Malka, V. & Mora, P. (2006). Proposed scheme for compact GeV laser plasma accelerator. *Laser Part. Beams* **24**, 255–259.

Maiorov, E.V., Okorokov, V.V. & Sveshnikova, N.V. (2004). Acceleration by nonuniform stochastic fields. Preprint 9-04. Moscow: Institute of Theoretical and Experimental Physics.

Mangles, S.P.D., Walton, B.R., Najmudin, Z., Dangor, A.E., Krushelnick, K., Malka, V., Manclossi, M., Lopes, N., Carias, C., Mendes, G. & Dorchies, F. (2006). Table-top laser-plasma acceleration as an electron radiography source. *Laser Part. Beams* **24**, 185–190.

Nakamura, T., Sakagami, H., Johzaki, T., Nagatomo, H. & Mima, K. (2006). Generation and transport of fast electrons inside cone targets irradiated by intense laser pulses. *Laser Part. Beams* **24**, 5–8.

Nickles, P.V., Ter-Avetisyan, S., Schnuerer, M., Sokollik, T., Sandner, W., Schreiber, J., Hilscher, D., Jahnke, U., Andreev, A. & Tikhonchuk, V. (2007). Review of ultrafast ion acceleration experiments in laser plasma at Max Born Institute. *Laser Part. Beams* **25**, 347–363.

Niu, H.Y., He, X.T., Qiao, B. & Zhou, C.T. (2008). Resonant acceleration of electrons by intense circularly polarized Gaussian laser pulses. *Laser Part. Beams* **26**, 51–59.

Rousseaux, C., Amiranoff, F., Labaune, C. & Matthieussent, G. (1992). Suprathermal and relativistic electrons produced in laser-plasma interaction at 0.26, 0.53, and 1.05 μm laser wavelength. *Phys. Fluids B* **4**, 2589–2595.

Sakagami, H., Johzaki, T., Nagatomo, H. & Mima, K. (2006), Fast ignition integrated interconnecting code project for cone-guided targets. *Laser Part. Beams* **24**, 191–198.

Sentoku, Y., Bychenkov, V.Y., Flippo, K., Maksimchuk, A., Mima, K., Mourou, G., Sheng, Z.M. & Umstadter, D. (2002). High-energy ion generation in interaction of short laser pulse with high-density plasma. *Appl. Phys. B* **74**, 207–215.

Sheng, Z-M., Mima, K., Zhang, J. & Meyer-ter-Vehn, J. (2004). Efficient acceleration of electrons with counterpropagating

intense laser pulses in vacuum and underdense plasma. *Phys. Rev. E* **69**, 016407-1/016407-12.

YIN, L., ALBRIGHT, B.J., HEGELICH, B.M. & FERNANDEZ, J.C. (2006). GeV laser ion acceleration from ultrathin targets: The laser break-out afterburner. *Laser Part. Beams* **24**, 291–298.

YU, W., YU, M.Y., XU, H., TIAN, Y.W., CHEN, J. & WONG, A.Y. (2007). Intense local plasma heating by stopping of ultrashort ultraintense laser pulse in dense plasma. *Laser Part. Beams* **25**, 631–638.

ZHANG, P., SALEH, N., CHEN, S., SHENG, Z.M. & UMSTADTER, D. (2003). Laser-energy transfer end enhancement of plasma waves and electron beams by interfering high-intensity laser pulses. *Phys. Rev. Lett*. **91**(22), 225001-1/225001-4.

ZVORYKIN, V.D., DIDENKO, N.V., IONIN, A.A., KHOLIN, I.V., KONYASHCHENKO, A.V., KROKHIN, O.N., LEVCHENKO, A.O., MAVRITSKII, A.O., MESYATS, G.A., MOLCHANOV, A.G., ROGULEV, M.A., SELEZNEV, L.V., SINITSYN, D.V., TENYAKOV, S.Y., USTINOVSKII, N.N. & ZAYARNYI, D.A. (2007). GARPUN-MTW: A hybrid Ti:Sapphire/KrF laser facility for simultaneous amplification of subpicosecond/nanosecond pulses relevant to fast-ignition ICF concept. *Laser Part. Beams* **25**, 435–451.

https://doi.org/10.1017/S0263034608000566 Published online by Cambridge University Press